Mathematical and Computational Applications

MDPI

Article

Deep Convolutional Neural Network for Detection and Prediction of Waxy Corn Seed Viability Using Hyperspectral Reflectance Imaging

Xiaoqing Zhao [1], Lei Pang [2], Lianming Wang [1], Sen Men [3,4] and Lei Yan [1,*]

[1] School of Technology, Beijing Forestry University, Beijing 100083, China
[2] Institute of Artificial Intelligence in Sports, Capital University of Physical Education and Sports, Beijing 100191, China
[3] College of Robotics, Beijing Union University, Beijing 100020, China
[4] Beijing Engineering Research Center of Smart Mechanical Innovation Design Service, Beijing Union University, Beijing 100020, China
* Correspondence: mark_yanlei@bjfu.edu.cn

Abstract: This paper aimed to combine hyperspectral imaging (378–1042 nm) and a deep convolutional neural network (DCNN) to rapidly and non-destructively detect and predict the viability of waxy corn seeds. Different viability levels were set by artificial aging (aging: 0 d, 3 d, 6 d, and 9 d), and spectral data for the first 10 h of seed germination were continuously collected. Bands that were significantly correlated (SC) with moisture, protein, starch, and fat content in the seeds were selected, and another optimal combination was extracted using a successive projection algorithm (SPA). The support vector machine (SVM), k-nearest neighbor (KNN), random forest (RF), and deep convolutional neural network (DCNN) approaches were used to establish the viability detection and prediction models. During detection, with the addition of different levels, the recognition effect of the first three methods decreased, while the DCNN method remained relatively stable (always above 95%). When using the previous 2.5 h data, the prediction accuracy rate was generally higher than the detection model. Among them, SVM + full band increased the most, while DCNN + full band was the highest, reaching 98.83% accuracy. These results indicate that the combined use of hyperspectral imaging technology and the DCNN method is more conducive to the rapid detection and prediction of seed viability.

Keywords: hyperspectral imaging; deep convolutional neural network; waxy corn seeds; viability detection

Citation: Zhao, X.; Pang, L.; Wang, L.; Men, S.; Yan, L. Deep Convolutional Neural Network for Detection and Prediction of Waxy Corn Seed Viability Using Hyperspectral Reflectance Imaging. *Math. Comput. Appl.* **2022**, *27*, 109. https://doi.org/10.3390/mca27060109

Academic Editor: Leonardo Trujillo

Received: 11 November 2022
Accepted: 12 December 2022
Published: 14 December 2022

1. Introduction

Seeds need to mature naturally before they can be stored for future sowing and other needs, and seed germination and viability are the major determinants of crop productivity. There are many factors (temperature, humidity changes, etc.) that will cause seeds to lose viability during storage [1] by changing the internal components of the seed and impacting subsequent germination, root growth, and development. Highly vigorous seeds are vital for farmers' production activities or commercial sale by seed companies [2].

Corn is currently one of the most cultivated food crops in the world [3]. Compared with traditional food crops such as rice and wheat, it has strong drought resistance, cold resistance, and excellent environmental adaptability. Waxy corn, a common type of corn mutation controlled by a recessive mutation gene, has a gene located on chromosome 9 that functions to inhibit the activity of granular coagulative starch synthetase. Moreover, the content of the nutrient components in waxy corn is higher than that of the nutrient components in ordinary corn. Like ordinary corn, the germination ability of waxy corn seeds is often lost during storage, which directly affects yield. Therefore, it is of great practical

significance to study methods of seed viability detection for distinguishing between high- and low-viability seeds.

The methods commonly used to identify seed viability are biological and chemical [4], including standard germination experiments and TTC quantitative assays, among various others. Although these methods are effective, they are characterized by tedious operations, long cycles, and damage to seeds. In recent years, physical detection methods, such as the conductivity method and infrared thermal imaging technology [5], have attracted much attention because of their rapid and non-destructive detection, but these methods still are limited by insufficient detection accuracy or an inability to detect in large quantities. In addition to the previously mentioned methods, near-infrared spectroscopy can analyze material changes in samples during seed aging and germination through transmission or reflection spectroscopy, and it is widely used in the detection of seed viability because of its rapidity and convenience [6]. However, near-infrared spectroscopy is based on point scanning, so it cannot provide a comprehensive analysis of sample information and is not suitable for data acquisition from a large number of samples.

Artificial accelerated aging tests have been used as a general method to simulate longer seed aging processes in a short period and has been important in research related to seed viability detection [7,8].

Hyperspectral imaging technology involves a unified image spectrum [9] which contains many bands and has high image resolution, and it can decrease the measured error caused by the uneven distribution of components in the sample by pixel average. Hyperspectral imaging technology combines imaging technology and spectroscopy technology. It can scan a large number of samples at one time and obtain complete sample information through images, thus overcoming the limitations of traditional spectroscopy technology, which usually only measures the local information of a single sample. As a technology that combines the advantages of traditional imagery and spectroscopic technology, the images it produces can help visualize samples [10] and the spectra can reflect the chemical composition of each part of the substance [11]. This method has been widely applied in the nondestructive testing of agricultural products and foods, such as in the prediction of the early decay of citrus [12] and black tea quality [13]. Extensive research has also been carried out on seed internal component prediction [14], classification [15], and lesion determination [16]. Furthermore, Kandpal et al. [17] quantified melon seed viability and vigor as high as 94.6% using near-infrared hyperspectral imaging technology and a partial least squares discriminant analysis (PLS-DA). After removing redundant information through feature selection, Li et al. [18] combined a support vector machine (SVM) approach with adaptive boosting to achieve 100% recognition of four viability grade soybean seeds. Hyperspectral imaging technology was also applicable to the discrimination of three different degrees of frozen corn seed viability with an accuracy rate of over 90% [19].

The deep convolutional neural network (DCNN) is one of the most representative neural networks in the field of deep learning technology, and it has led to many breakthroughs in image analysis and processing. At present, the DCNN has been studied in many scientific fields [20,21], especially in pattern classification. Since the network avoids the complex preprocessing of the image, it can directly input the original image. When applied together with hyperspectral imaging technology, both spectral and image data are available, and this has been used to classify similar samples. For instance, seven cotton seed varieties can be better distinguished by a DCNN than by an SVM, whether it is a full band or characteristic band dataset [22].

In this study, spectral data were collected for the germination (10 h) of seeds of different viability grades after artificial aging. Before applying the SVM, k-nearest neighbor (KNN), random forest (RF), and DCNN approaches to establish viability detection models, dimensionality reduction was performed based on a successive projection algorithm (SPA) and component-related bands. Unlike previous studies, this paper separates the steps of seed viability detection and prediction to reduce the original standard germination time

(7 days) and increase the detection speed. As shown through changes in spectral reflectance over time, a more accurate prediction of seed viability can be achieved in a shorter time.

2. Materials and Methods

Figure 1 is the overall flowchart of this study, including the entire process of seed aging, spectrum extraction, component detection, feature band selection, viability detection, and prediction model establishment.

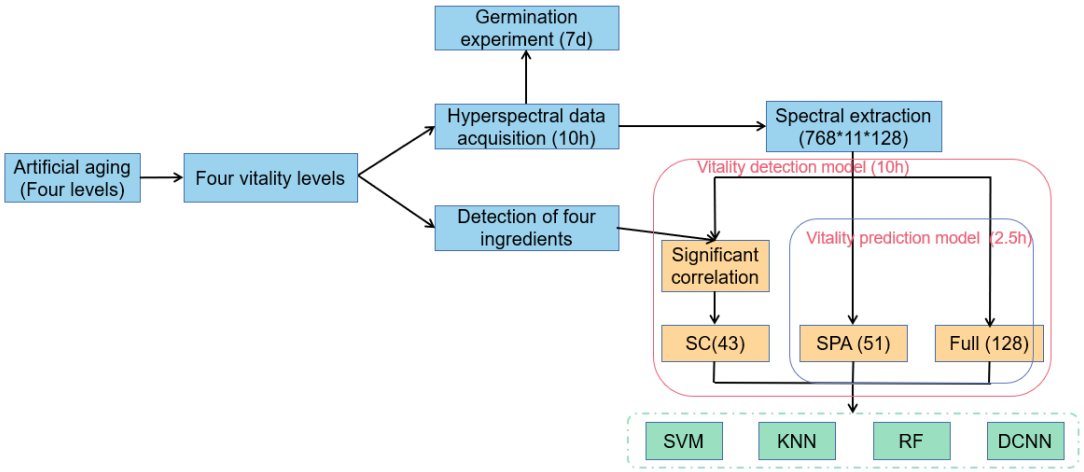

Figure 1. Flow chart for detecting and predicting the viability of waxy corn seeds using hyperspectral imaging.

2.1. Sample Preparation

Zhongpintian F1, a variety of waxy corn, was purchased from the Beijing Seed Market. After the initial selection, the seeds were divided into four groups for high-temperature treatment to achieve artificial aging. The temperature of the aging box, model LH-80 (Top Cloud-Agri Technology Co., Hangzhou, China), was set to 45 °C and the relative humidity was 99% [23]. One group was not treated with high temperature and served as the control group. The remaining three groups were placed in the aging box for 3 d, 6 d, and 9 d [24]. After aging, the seeds were dried in an incubator at 25 °C to restore their original weight. For each aging grade of waxy corn seeds, 300 g samples were randomly weighed to measure the internal moisture, starch, protein, and fat content of the seeds, and then 192 samples were randomly selected from the remaining seeds for spectrum collection and standard germination experiments. The total number of seeds used for data collection was 768.

The detection of internal substance content in different viability levels was mainly used to explore the effect of artificial aging on the internal components of the seeds. China's Tianyuan Yingkang Inspection and Evaluation Company helped to complete this work. For moisture detection, the direct drying method [25] was used; the Soxhlet extraction method [26] was used for fat detection; the Kjeldahl method was used for protein [27]; and an acid hydrolysis method was used for starch [28].

2.2. Standard Germination Experiment

In general, for germination purposes, it is appropriate to soak hard corn seeds for 8–10 h. Since our seeds were not completely immersed in water, but kept moist by wet filter paper, we chose 10 h as the length of time to soak the seeds for germination. While collecting 10-h hyperspectral data for seeds of different viability grades, standard germination experiments were performed according to GB/T requirements [29] and continued for 7 days. All samples were placed between two layers of filter paper, as shown in Figure 2a, with the edges of the filter paper immersed in water and kept moist in a 25 °C incubator. Germination was checked daily. If the shoot length exceeded 1 cm, the waxy corn seed was

considered germinated; conversely, it was recorded as not germinated if the shoot length was less than 1 cm [23,30]. In addition to germination percentage (GP) and average shoot length (s), the following three indicators together also indicate seed germination ability.

$$\begin{aligned} &\text{Germination index (GI)} = \sum (Gt/Dt) \\ &\text{Vitality Index (VI)} = \text{GI} \times s \\ &\text{Average Germination Days (AGD)} = \sum (Gt \times Dt)/\sum Gt \end{aligned} \tag{1}$$

where Gt is the number of germinations per day at the specified time and Dt is the number of germination days in response. The duration of this study was 7 days.

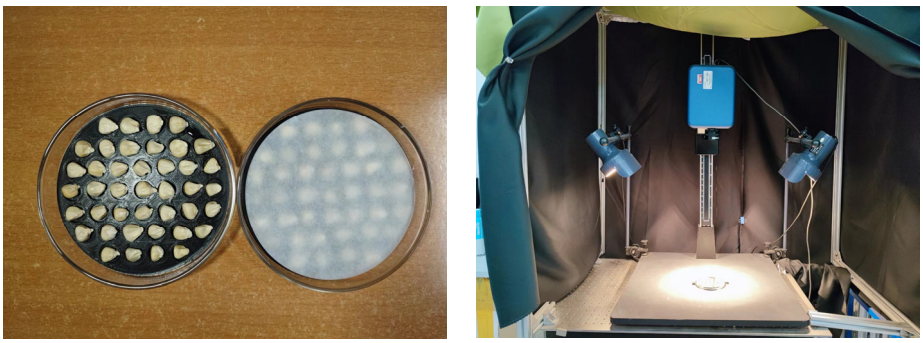

(**a**) (**b**)

Figure 2. The experimental processes. (**a**) Bud stimulating experiment; (**b**) spectral acquisition experiment.

Table 1 lists the germination results of all the waxy corn seeds. It can be seen that with the increase in artificial aging time, except for AGD, which first decreased and then increased, other indicators increased first and then decreased, which may reflect the fact that the ability of the seeds to germinate was enhanced after 3 days of treatment at 45 °C. The results indicate that the artificial aging method can change the physiological and biochemical indices of seeds, and the different viability levels set (named A, B, C, and D) according to aging time and germination made the simulation of natural aging more comprehensive.

Table 1. Germination test to determine seed viability in all groups.

Aging Time (d)	Vitality Level	Number of Samples	Viable Seeds	GP (%)	s (cm)	GI	VI	AGD (d)
0	A	192	172	89.6	2.59	41.46	107.38	4.7
3	B	192	180	93.8	2.63	49.99	131.47	3.9
6	C	192	114	59.4	1.10	26.03	28.63	5
9	D	192	33	17.2	0.21	6.45	1.35	5.5
Total		768	499	65	1.63	30.98	67.21	4.8

2.3. Hyperspectral Image Acquisition and Correction

A hyperspectral imager adopts line scanning to collect hyperspectral data from samples. The hyperspectral imaging system used in this experiment included a SOC710VP visible/near-infrared hyperspectral imaging spectrometer (Surface Optics Corp., San Diego, CA, USA), two 250 W Pro-light halogen lamps for lighting (OSRAM GCA; Sylvania, Gloucester, MA, USA), and a computer. The spectrometer has a spectral range of 378 nm to 1042 nm with 128 bands, a spectral resolution of 4.6875 nm, and a resolution of 520 × 696 for images. The Petri dish with corn seeds was placed 40 cm from the lens, directly below the spectrometer, as shown in Figure 2b, and the experiment was performed in a dark room to ensure that there was no external light. Example hyperspectral images of four kinds of corn seeds with different vitality levels are shown in Figure 3. The black reference image (I_{dark}) was obtained by covering the entire lens with a black cap, and the white reference

image (I_{white}) was obtained by using a white Teflon tile with nearly 100% reflectance. The correction to the original image (I_{raw}) was calculated using Equation (2).

$$I = \frac{I_{raw} - I_{dark}}{I_{white} - I_{dark}} \tag{2}$$

To study the germination process of waxy corn seeds with different viability levels using hyperspectral imaging, the data collection process lasted for 10 h at 0.5 h intervals. This process was carried out simultaneously with the first 10 h of the standard germination experiment, so a regular quantitative water supplement was required to ensure accurate germination.

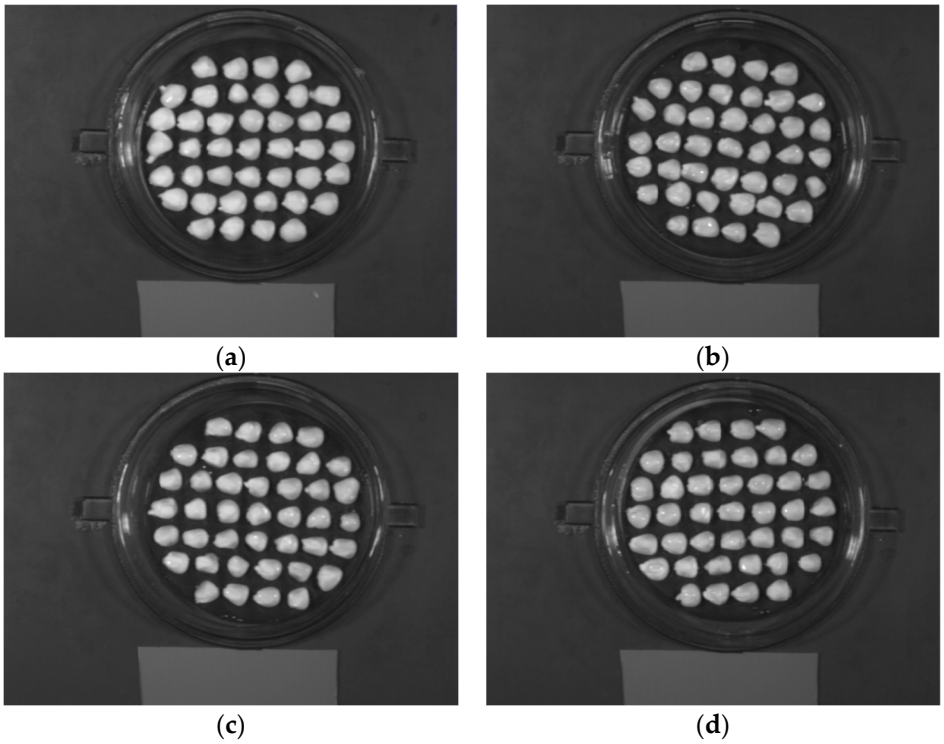

Figure 3. The example hyperspectral images of (**a**) A; (**b**) B; (**c**) C; (**d**) D.

2.4. Spectra Extraction

Using a simple threshold as the average of background pixels and waxy corn seed pixels, the calibrated hyperspectral image was segmented to eliminate the background effect and facilitate seed visualization. Due to the large number of pixel points in the seed region, the complete region of each seed was taken as the region of interest (ROI), and the spectrum of each seed was extracted from the ROI. The obtained spectral information could be used to reflect the spectral situation of the whole seed and also facilitate the subsequent computational analysis. In this study, a threshold segmentation band of 738.47 nm was selected, and the difference between the seed background reflectance reached a maximum at this position. By thresholding the grayscale image in this band to create a binary image mask ("1" for the seed region and "0" for the background region), it was possible to effectively segment the true area of the maize seed from the 128 wavelengths of the hypercube and achieve the purpose of background segmentation. Finally, the average spectrum of the seeds was calculated according to the average of all the pixel intensity values in the 128 bands of each ROI. The spectrum of each seed at each germination time was then used in the model.

2.5. Multivariate Data Analysis

To further study the feasibility and ability of the DCNN to detect and predict the viability of waxy corn seeds based on hyperspectral data, the SVM, KNN, and RF approaches were compared. Before modeling, an SPA, which could be combined with the four discriminative models, was used to extract feature bands to remove redundant information and reduce the high dimensionality.

In recent years, researchers have used SPAs to select effective wavelengths when detecting the content of important components in crops and foods with spectral analysis techniques [10,31]. SPAs can effectively eliminate the co-linearity among wavelength variables and minimize the co-linearity between vectors. This method not only reduces the complexity of the model, but also improves its speed and efficiency, and it has achieved good results in the selection of sampling wavelengths.

The basic SVM model is a linear classifier with the largest interval defined in the feature space. The learning strategy is to maximize the interval, which can be formalized as a problem for solving convex quadratic programming and is also equivalent to minimizing the regularized hinge loss function [32]. Based on the limited sample information, the best compromise is sought between the complexity of the model (that is, the learning accuracy of a specific training sample) and the learning ability (that is, the ability to identify any sample without error) to obtain the best generalization ability. The kernel technique of the SVM model makes it a substantially nonlinear classifier [33], and the radial basis kernel (RBF) used in this research is one of these. In this model, the penalty coefficient I and the kernel parameter (g) were determined by grid search in the range of 2–8–28.

The KNN classification algorithm is one of the commonly used methods in data mining classification technology. It is intuitively expressed that each sample can be represented by its nearest k neighbors [34]. The specific steps are as follows: calculating the distance between the test data and each training datum; sorting according to the increasing relationship between distances; selecting the k points with the smallest distance; determining the frequency of occurrence of the category in which the first k points are located; returning the category with the highest occurrence frequency as the prediction classification of the test data. If the value of k is too small, it is extremely susceptible to the influence of noise, and the approximation error of learning will increase when the value of k is too large. In this study, cross-validation was used to calculate the error rate of the classifier for each k, and then select the k that produced the smallest error rate.

RF is a flexible and easy-to-use machine learning algorithm that can get good results in most cases even without hyperparameter tuning [35]. The principle is to build a forest in a random manner, which consists of many decision trees, with no correlation between each decision tree. When a new input sample is entered, each decision tree will judge the sample separately, and the type selected most will serve as the predicted sample type. Because its training can be highly parallelized, it has the advantage of a fast large sample training speed in the era of big data. The node value represented by mtry, a key parameter, is usually set as the root mean square of the number of variables.

Convolutional neural networks (CNNs) have unique advantages in image processing [36] due to their special structure, which incorporates local weight sharing, and their layout is closer to those of actual biological neural networks. Weight sharing reduces the complexity of the network, especially the multidimensional input vector images that can be directly inputted to avoid the complexity of data reconstruction during feature extraction and classification. A DCNN is mainly composed of an input layer, a convolutional layer, an activation function, a pooling layer, a fully connected layer, and an output layer [37], and it can directly take pictures as the input of the network. A convolution module usually contains one or more convolutional layers and an activation function. The neuron is only connected to its neighboring upper-layer neurons, and the final global features are formed by combining the learned local features. The same convolution kernel uses the same weight parameter when operating on different local receptive fields, and this can reduce the number of parameter calculations. The pooling layer reduces the feature size of the picture

through the pooling process, and this can effectively remove the problem of a large number of calculations caused by the result of the previous layer as input. The fully connected layer is similar to the fully connected module of the traditional neural network, and it completes the classification task. A DCNN perfectly integrates feature learning, deep-level feature extraction, dimensionality reduction, and final classification into one system.

For the waxy corn spectral data, a one-dimensional deep convolutional neural network was used. The structure of the DCNN in this paper is shown in Figure 4. The input of the DCNN was a 128 × 1 vector, which is the average spectrum of each seed. In addition to input and output, it included four convolution modules and three fully connected modules. The number of convolutional layer filters was different for each convolutional module and doubled as the module deepened. The size of the convolution kernel was set to 1 × 3, and the stride and padding were both 1. The pooling layer employed the maximum pooling method with a kernel size of 2 and a step size and padding of 1. In the fully connected module, to prevent overfitting during the training process, the dropout method was used (p = 0.3), and the fully connected layer was able to learn the combination of features extracted by the convolutional layer. For the convolutional layers and fully connected layers, the exponential linear unit (ELU) and rectified linear unit (RELU) were used as activation functions. In each model, the learning rate was fixed to 10^{-4} [38], and the size of the batch was run many times according to the exponential power of 2 to match the 2n storage form of computer characters. The output shape and param of each layer of 1DCNN are shown in Table 2.

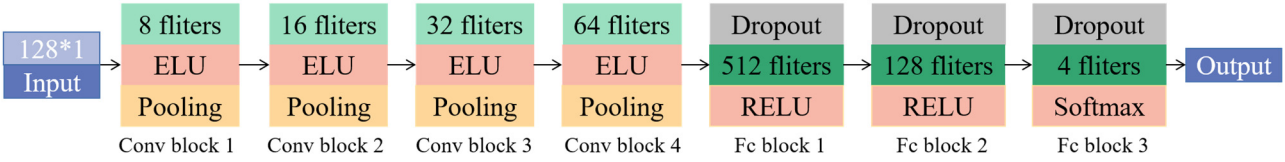

Figure 4. The structure of the DCNN used in this study.

Table 2. The output shape and params of the the DCNN model.

Layer (Type)	Output Shape	Param
Input	(128, 1)	0
Conv1D_1	(128, 8)	32
MaxPooling1D_1	(64, 8)	0
Conv1D_2	(64, 16)	400
MaxPooling1D_2	(32, 16)	0
Conv1D_3	(32, 32)	1568
MaxPooling1D_3	(16, 32)	0
Conv1D_4	(16, 64)	6208
MaxPooling1D_4	(8, 64)	0
Flatten	(512)	0
Dropout_1	(512)	0
Dense_1	(512)	262,656
Dropout_2	(512)	0
Dense_2	(128)	65,664
Ddropout_2	(128)	0
Dense_3	(4)	516
Total params	/	337,044

2.6. Software

The spectral extraction of a single waxy corn seed based on hyperspectral images in this study was performed on Matlab 2019a (The Math-Works, Natick, MA, USA), and Python 3.6 with Pycharm implemented was used for the advanced feature selection and four discriminative models. Among them, a deep convolutional neural network based on the Keras framework was built to program the DCNN model.

3. Results and Discussion

3.1. Overview of Waxy Corn Seed Spectra

Figure 5a shows the change in the average spectrum of the seeds of grade B (as an example) during the 10 h germination time. During the germination, at 0.5 h intervals, the spectra showed similar trends, and the reflectance changed only slightly. However, it can be seen that as the germination time increased, the overall reflection spectrum curve decreased. The difference between 0 h and 10 h germination was the most apparent. This shows that it is feasible to study the process of seed germination with hyperspectral imaging technology, which can represent the difference in average reflectance.

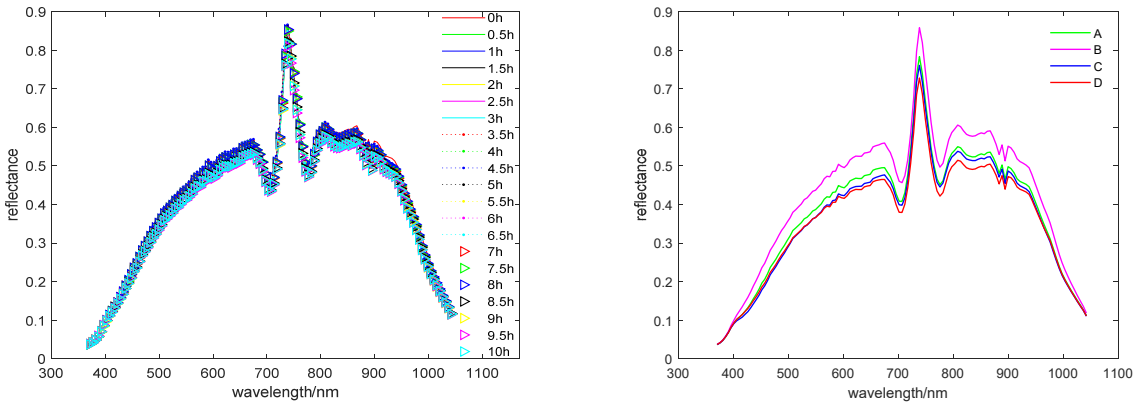

(**a**) (**b**)

Figure 5. The average spectrum of (**a**) grade B seeds within 10 h of germination; (**b**) the four viability grade seeds over the entire process.

The four curves in Figure 5b are the average spectra of four aging grade seeds across the entire germination time (10 h). The reflection spectra of seeds of different viability grades in the wavelength range shared the same peak and valley positions, but there were also some differences reflected in the values. These differences may be attributed to discrepancies in the internal composition and surface information of seeds of different viability [39]. For example, the absorption peak at 730 nm has been reported to be related to C–H stretching resulting from the absorption by CH3 [40]. The peak at 960 nm was related to the second overtone of the O–H bond in water [41]. The average spectra of seeds aged in grade C and grade D still overlapped significantly in some bands, so a more accurate multivariate analysis was necessary.

3.2. Detection Results of Seed Viability under Different Models with Full-Wavelength Data

The spectrum data were collected every 0.5 h for 10 h, 21 times in total. The number of samples for each category was 192, the total amount of sample data for each category was $21 \times 192 = 4032$, and the data size was 4032×128. The seed germination data of the four viability grades were randomly divided into a training set and a test set according to a 3:1 ratio, 10% of the training set was randomly selected as the validation set, and the final result was obtained by the averaging of five randomized trials. Three typical machine learning algorithms (SVM, KNN, RF) and a deep convolutional neural network (DCNN) were used to build the model on 128 bands to analyze the effect of different discriminant models on waxy corn seed viability detection. The experiments were conducted on a system with an Intel Core i7 8500U processor. The results are given in Table 3 and reflect the specific parameter settings. During the modeling, the effect of each model was also compared with the increase in the number of viability levels. The first were grade A and grade D, and then grade B and grade C seeds were added. The accuracy rate of all model training sets was above 95%, but there were differences in the calculation time and accuracy of the test set.

Table 3. Identification results of waxy corn seed viability by different discrimination models in the whole band.

Number of Levels Included	Discriminant Model	Main Parameters	Training Set Accuracy	Test Set Accuracy	Time (s)
2	SVM	c = 2.0, g = 4.1	100%	96.24%	8.42
	KNN	K = 3	99.52%	93.5%	7.55
	RF	mtry = 11	100%	93.3%	7.81
	DCNN	lr = 10^{-4}, batchsize = 64	100%	98.20%	369.81
3	SVM	c = 3.0, g = 3.5	97.4%	95.30%	75.88
	KNN	K = 5	98.37%	92.77%	9.96
	RF	mtry = 11	100%	89.13%	13.16
	DCNN	lr = 10^{-4}, batchsize = 64	100%	98.35%	554.98
4	SVM	c = 3.1, g = 4.7	94.99%	92.34%	191.48
	KNN	K = 7	95.38%	86.95%	15.07
	RF	mtry = 11	100%	85.46%	17.41
	DCNN	lr = 10^{-4}, batchsize = 64	99.98%	97.47%	608.61

When only high-viability and low-viability seed data were input, the KNN and SVM results were similar, while the DCNN model had the best accuracy (more than 95%) after parameter optimization. In previous studies, many attempts have been made to detect two types of seeds with significantly different viability. Ambrose et al. [3] used PLS-DA for rapid viability testing of corn seeds before and after microwave heat treatment. The recognition effect of the SVM model on high-temperature heat damage and undamaged tomato seeds exceeded 96% [42]. The SVM model based on the RBF kernel can make full use of the non-linear hyperplane to classify complex data, but the accuracy rate declined by 0.94% and 3.90% based on 96.24% as the viability level added. The gap between the four types of simultaneous input was relatively small, and the overall accuracy of the KNN model based on distance discrimination was reduced by 6.55%. The correlation between any two trees in the RF increased, resulting in a large error rate, that is, the accuracy rate dropped the most (up to 7.84%). When only distinguishing high and low viability, the two were different in viability or spectral data, so machine learning algorithms can also achieve results similar to those achieved using a DCNN. However, the differences between the categories decreased as the level of viability increased, and there was more crossover and overlap during the germination process, which made it difficult to discriminate. For more complex seed spectral data, the abstract and invariant deep features extracted by a DCNN are more effective [43,44]. When distinguishing the three vitality levels, the DCNN model obtained the best accuracy rate of 98.35%. It can be seen from the confusion matrix (Figure 6) that when distinguishing four vitality levels, the features extracted from the convolution layer were not enough to distinguish all the categories, and the classification accuracy of the model decreased slightly. In terms of calculation time, the calculation time of DCNN model was much longer than that of the SVM, KNN, and RF algorithms, but the accuracy of the model was relatively high and stable. In addition, we can see from Figure 7 that the model has been fitted in about 200 iterations, which can further shorten the time in practical application in the future.

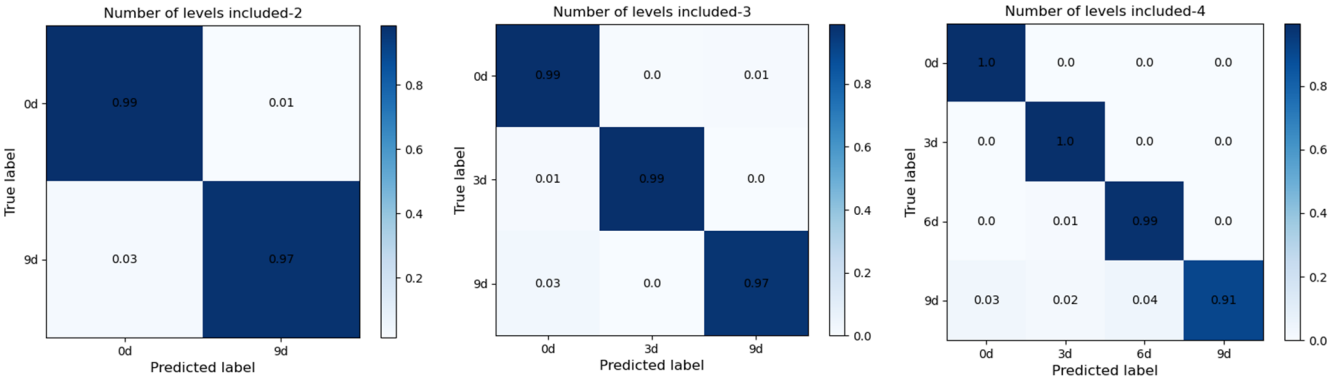

(**a**) (**b**) (**c**)

Figure 6. Confusion matrix based on the DCNN model. (**a**) Confusion matrix of prediction sets for two vitality levels; (**b**) confusion matrix of prediction sets for three vitality levels; (**c**) confusion matrix of prediction sets for four vitality levels.

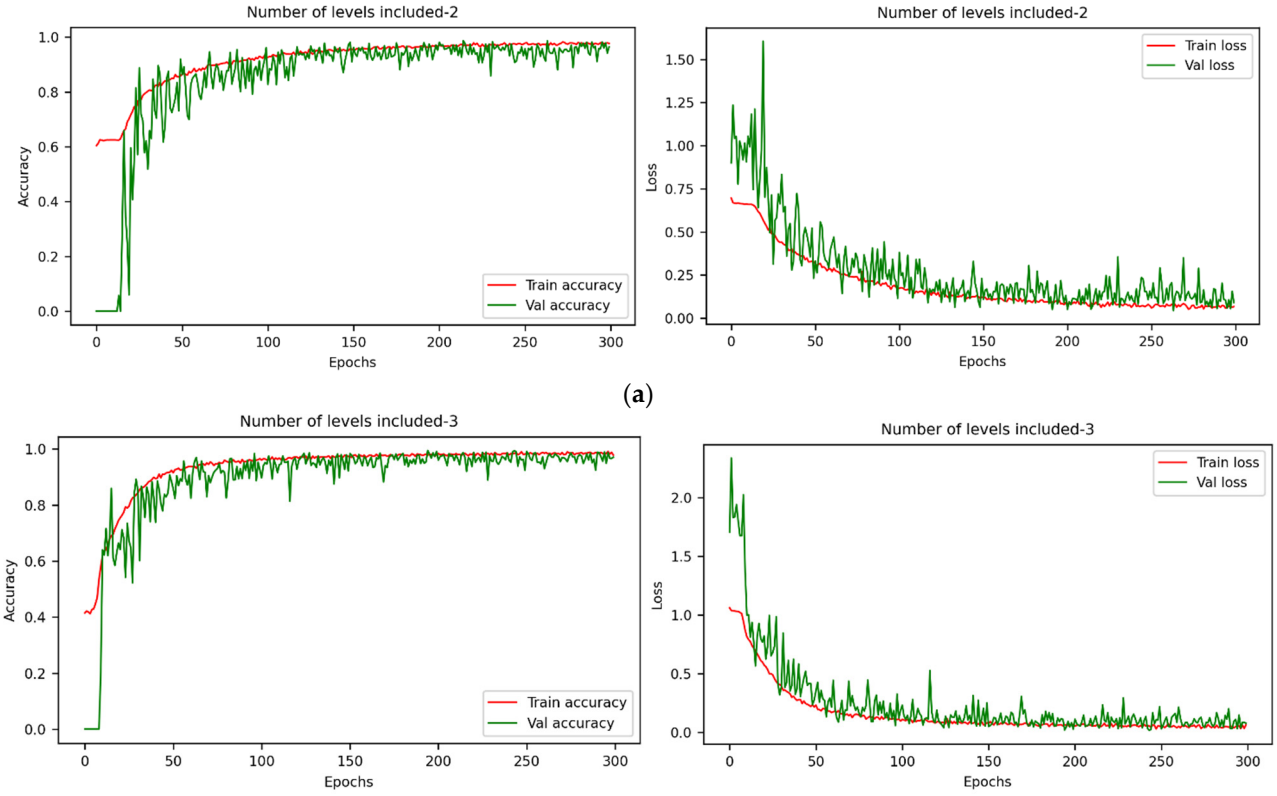

(**a**)

(**b**)

Figure 7. *Cont.*

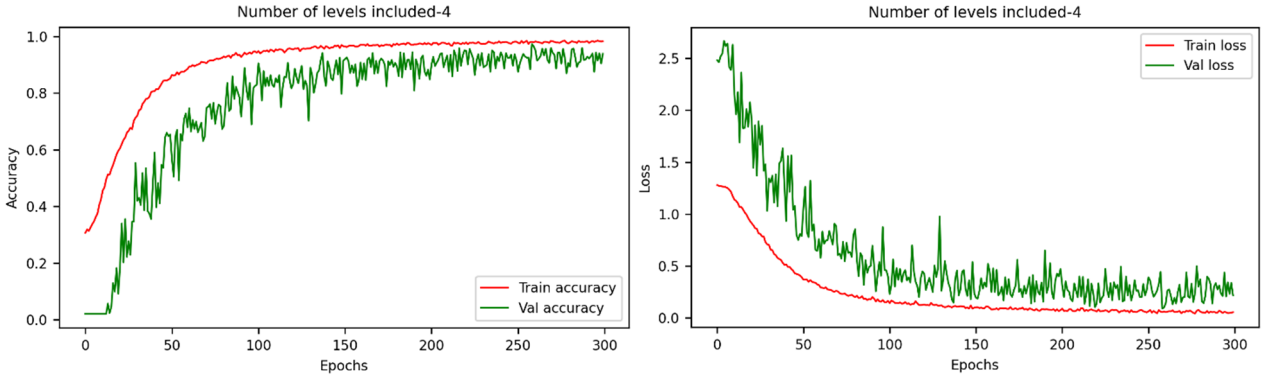

(**c**)

Figure 7. Training process of the DCNN model. (**a**) Iterative curves of training set and validation set for two vitality levels; (**b**) iterative curves of training set and validation set for three vitality levels; (**c**) iterative curves of training set and validation set for four vitality levels.

3.3. Chemical Composition Analysis and Characteristic Wavelength Selection

The test results for the component contents are given in Table 4. In light of the test results for internal moisture, fat, protein, and starch (Table 4), it can be concluded that artificial aging will change the content of some components in waxy corn seeds. As the aging time increased, the moisture content inside the seeds showed a downward trend, while the fat content fluctuated only slightly. Protein provides nitrogen for seed germination and seedling production and plays an important role in seed germination and embryo growth. Compared with normal seeds, aging reduces the protein content of waxy corn seeds. This may be due to the destruction of lysosomes in cells by peroxidation and the enrichment of corresponding enzymes, thereby enhancing the degradation of storage materials such as proteins [45]. Both α-amylase and β-amylase tended to decrease with the degree of aging [46,47]. However, in the early stage of aging, the amylase activity was still relatively high, and this can promote starch hydrolysis [48,49]. After 9 d of aging, the amylase activity was inhibited, delaying the decomposition of starch, and the starch content increased.

Table 4. Test results of the four components in different vitality grade seeds.

Sample Vitality Level	Content of Main Ingredients (g/100 g)			
	Moisture	**Fat**	**Protein**	**Starch**
Normal	9.70 ± 0.11^{a}	4.20 ± 0.03^{c}	11.1 ± 0.26^{a}	65.6 ± 1.25^{a}
Aging for 3 days	8.68 ± 0.07^{b}	4.30 ± 0.06^{b}	10.3 ± 0.10^{c}	36.0 ± 0.81^{c}
Aging for 6 days	8.10 ± 0.10^{c}	4.60 ± 0.11^{a}	10.6 ± 0.10^{b}	34.7 ± 0.70^{c}
Aging for 9 days	7.77 ± 0.24^{c}	4.50 ± 0.08^{a}	10.0 ± 0.03^{d}	43.3 ± 2.95^{b}

Values are means and standard deviations. Values followed by different superscripts in the column are significantly different ($p \leq 0.05$) from one another.

Therefore, based on the variability of the component content, the bands related to the components were selected using Pearson correlation coefficients [50] and then recombined into a new set for model establishment. As shown in Figure 8, when the correlation coefficient was > 0.8 and the *p*-value was < 0.05, the position of the characteristic band was marked on the correlation curve. A total of 43 relevant bands were extracted after the repeated bands were removed, among which the number of bands significantly related to starch was the highest. These bands mainly existed in the near-infrared band, which may have been due to the large proportion of starch in waxy corn seeds [51]. When the root mean square error (RMSE) was at a minimum, the SPA selected 51 wavelength bands as the optimal wavelength combination, and the results showed a relatively uniform distribution at 400–1000 nm. Table 5 shows the details related to component and feature selection.

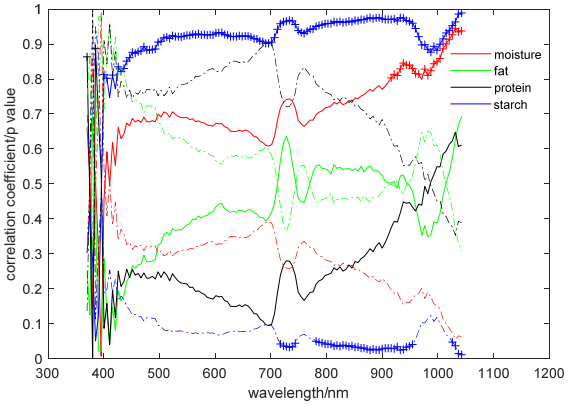

Figure 8. Correlation and *p*-value of the average spectrum and component content. The solid line represents the correlation curve and the dotted line is the p-value curve.

Table 5. Optimal bands extracted using an SPA and an SC algorithm.

Method of Choosing	Number of Bands	Wavelength (nm)
SC	43	717.2, 722.5, 727.8, 733.2, 738.5, 743.8, 781.2, 786.5, 791.9, 797.2, 802.6, 807.9, 813.3, 818.7, 824.1, 829.5, 834.8, 840.2, 845.6, 851.0, 856.4, 861.8, 867.2, 872.6, 878.1, 883.5, 888.9, 894.3, 899.8, 905.2, 910.6, 916.1, 921.5, 926.9, 932.4, 937.9, 943.3, 948.8, 954.3, 1025.7, 1031.2, 1036.8, 1042.3
SPA	51	410.8, 451.5, 487.4, 492.6, 502.9, 508.0, 513.2, 528.7, 533.8, 539.0, 544.2, 549.4, 554.6, 575.4, 580.6, 585.8, 596.2, 606.6, 638.1, 643.3, 653.8, 659.1, 664.4, 685.5, 706.6, 711.9, 733.2, 743.8, 754.5, 759.8, 765.1, 775.8, 781.2, 786.5, 791.9, 797.2, 807.9, 813.3, 818.7, 834.8, 856.4, 888.9, 890.9, 905.2, 910.6, 932.4, 937.9, 943.3, 948.8, 970.7, 976.2

3.4. Classification Results and Analysis of the Viability Detection Model Based on Optimal Band Spectra

A new viability detection model was established based on characteristic bands to simplify the complexity and improve the operating speed. These characteristic bands were combined and inputted into the SVM, KNN, RF, and DCNN models (as shown in Table 6). Confusion matrix and training process are shown in Figures 9 and 10. The results showed that the detection result of the SPA was better than that of the SC algorithm (within a 10% difference). Only the component detection data from the beginning of germination were used, but they did not extend through the entire germination process, so the accuracy of the SC algorithm may have been low. Although the number of the two bands was similar, the uniform distribution of the SPA features made the information acquisition of the original data more comprehensive. The SPA was able to use 51 bands to achieve similar or better results than all 128 bands. Among the three machine learning algorithms, the SPA effectively removed the influence of redundant band information and improved the recognition result [52]. The reduction in the data volume may have affected the extraction of deeper features, so there was a slight decrease in the DCNN model that was not much different from the former. In short, feature dimension reduction and combination optimization are of great significance to the establishment of a waxy corn seed viability detection model which can reduce the number of calculations and guarantee results close to the original data.

Table 6. Results of viability detection on characteristic bands.

Discriminant Model	Feature Selection Method (Number)	Main Parameters	Training Set Accuracy	Test Set Accuracy	Time (s)
SVM	SPA (51)	c = 1.7, g = 3.5	93.4%	86.56%	122.44
	SC (43)	c = 1.3, g = 1.8	82.92%	79.41%	144.51
KNN	SPA (51)	K = 4	95.34%	86.31%	5.22
	SC (43)	K = 4	89.07%	77.34%	5.16
RF	SPA (51)	mtry = 7	100%	86.6%	8.51
	SC (43)	mtry = 6	100%	83.28%	7.55
DCNN	SPA (51)	lr = 10^{-4}, batchsize = 32	99.74%	94.25%	509.32
	SC (43)	lr = 10^{-4}, batchsize = 32	99.57%	91.16%	466.34

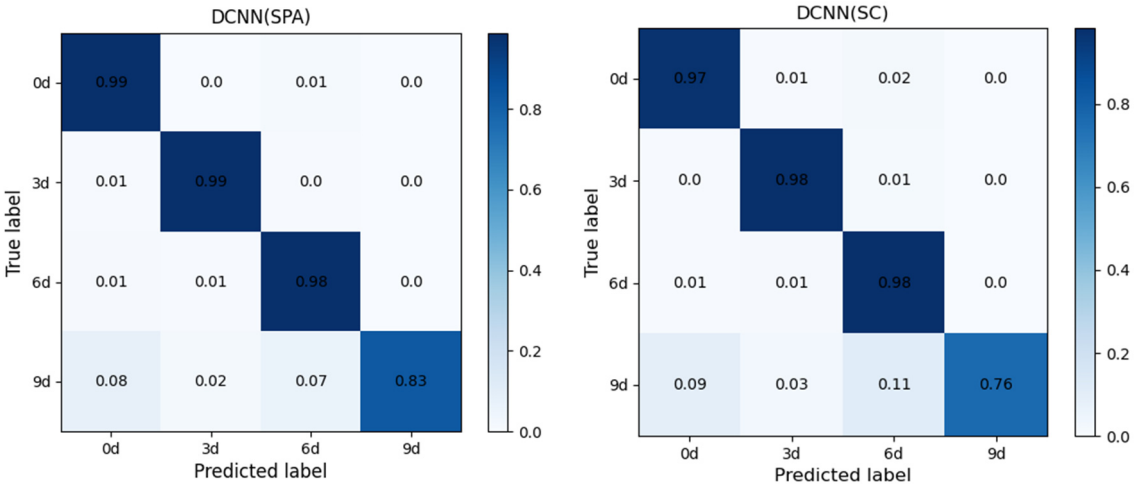

(**a**) (**b**)

Figure 9. Confusion matrix based on characteristic wavelength. (**a**) Confusion matrix based on SPA; (**b**) confusion matrix based on SC algorithm.

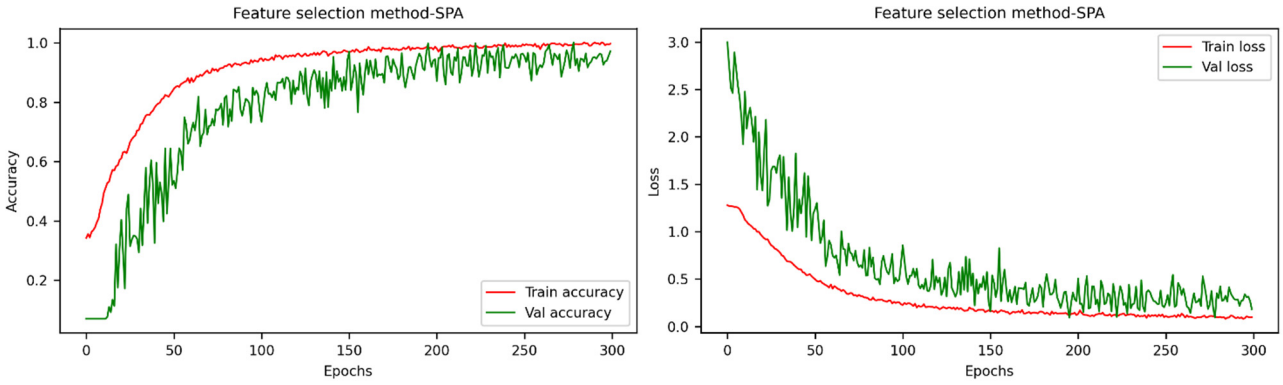

(**a**)

Figure 10. *Cont.*

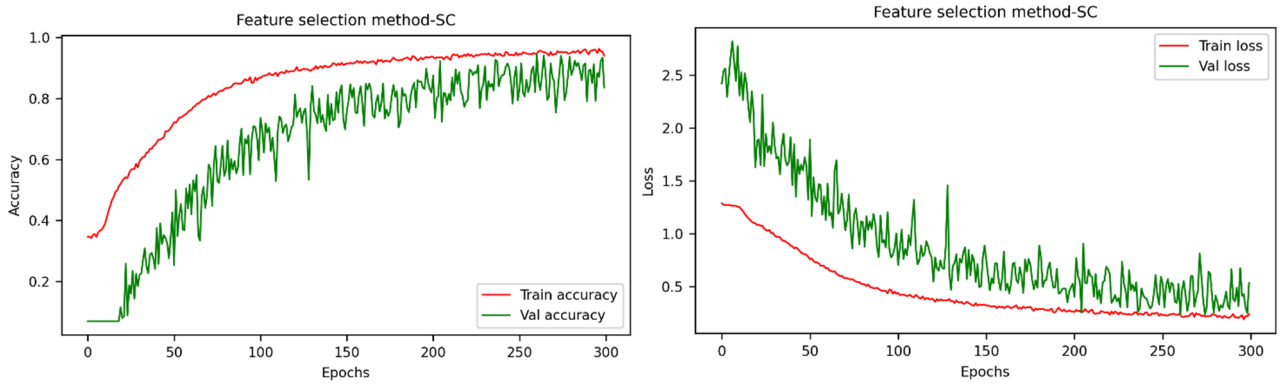

(**b**)

Figure 10. Training process of DCNN model based on characteristic wavelength. (**a**) Iterative curves of training set and validation set based on SPA; (**b**) iterative curves of training set and validation set based on SC algorithm.

3.5. Seed Viability Prediction Based on the Optimal Model

Although a good detection model has been established using data from the first 10 h of germination, data collection was still a relatively complicated and time-consuming process. The original data were used to construct the curve of the spectral reflectance of seeds with different viability grades within 10 h. The process of establishing this relationship was as follows: (1) determine the location of the 51 bands extracted using the SPA and the corresponding weight coefficients of each band; (2) find the reflectance corresponding to these bands on each original spectral curve; (3) calculate all weighted averages of band weight and reflectivity; (4) repeat four times using the data for the four seed viability levels. Figure 11 shows the final time–reflectance curve. The reflectivity of each viability level changed greatly during the germination process, especially the seeds of grade B. From 1–2.5 h of germination, the grade C and grade D seed curves intersected, which introduced some uncertainty. Finally, the data from the first 2.5 h were used as prediction data to achieve a more accurate and stable viability prediction.

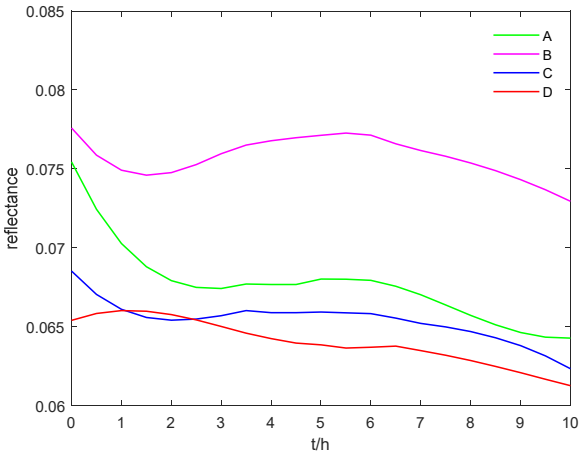

Figure 11. Curves of the average spectra of different grade seeds with germination time.

The viability prediction results of different discrimination models combined with the SPA are shown in Figure 12, and the activity detection results are also presented to make the comparison effect more intuitive. Vital prediction model results were better than the detection model results in most cases. This was especially reflected in the RF and DCNN models. The RF model was nearly 10% higher, and DCNN + full band achieved the best result (98.83%). Although the prediction accuracy of some models was not as good as their detection accuracy, the gap was small. The above results show that it was an effective

and meaningful way to distinguish between seed viability detection and prediction. It is feasible to predict the viability of waxy corn seeds in a shorter time, and this can reduce the workload and enhance the detection ability overall.

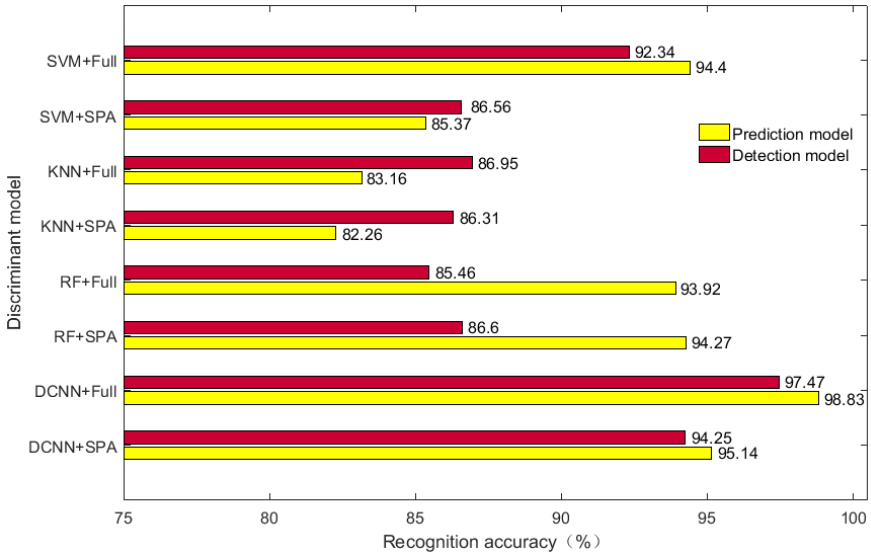

Figure 12. Viability prediction results of different combination models.

4. Conclusions

In this paper, hyperspectral imaging technology and different discrimination models were used to distinguish and predict the viability of waxy corn seeds. The data collection lasted for 10 h and the data were used to study the seed germination process for seeds of four different viability levels. Based on the full band (128 features), the SPA selection (51 features), and the SC algorithm selection (43 features), the discriminant models of the machine learning methods (SVM, KNN, RF) and deep learning method (DCNN) were established. With the increase in samples with different activity levels, the DCNN method showed better stability than the other three methods. Since the component detection does not extend to the whole germination process, the SPA can achieve a closer effect than the SC algorithm on the full band with fewer bands. The data from the first 2.5 h were selected as the prediction group according to the time-varying curve of seed spectral reflectance with different viability levels. The establishment of the final viability prediction model indicated the feasibility and advantages of short-term detection, and its results were significantly improved over the detection model, in which DCNN + full band and DCNN + spa reached 98.83% and 95.14% accuracy, respectively. The experimental results showed that the combination of hyperspectral imaging and a DCNN have great potential for seed viability detection, and that the differentiation of viability prediction can help reduce the detection time and increase accuracy. This can help farmers determine the viability of seeds in advance before actual planting. In future research, various deep learning networks can be used in conjunction with spectra or images to make better use of time series. Additionally, longer data collection may be more conducive to building higher-precision viability prediction models in a shorter time. The changes in the internal components of the seeds are particularly important in this process and can guide the study of the germination process of the seed.

Author Contributions: Methodology, X.Z. and L.P.; software, X.Z. and L.P.; writing—original draft, X.Z. and L.P.; supervision, L.Y.; project administration, L.W. and L.Y.; validation, S.M. All authors have read and agreed to the published version of the manuscript.

Funding: This research was funded by (1) the Opening Foundation of Key Lab of State Forestry Administration on Forestry Equipment and Automation (Grant BFUKF202220); (2) the General Program

of Science and Technology Development Project of the Beijing Municipal Education Commission of China (Grant KM201911417008); (3) the National Natural Science Foundation of China (Grant No. 31770769).

Data Availability Statement: The raw data used in our research cannot be shared at this time as the data also form part of an ongoing study.

Conflicts of Interest: The authors declare no conflict of interest.

References

1. De Bittencourt, S.R.M.; Grzybowski, C.R.D.S.; Panobianco, M.; Vieira, R.D. Metodologia alternativa para condução do teste de envelhecimento acelerado em sementes de milho. *Ciênc. Rural* **2012**, *42*, 1360–1365. [CrossRef]
2. Williams, P.; Manley, M.; Fox, G.; Geladi, P. Indirect Detection of *Fusarium Verticillioides* in Maize (*Zea mays* L.) Kernels by near Infrared Hyperspectral Imaging. *J. Near Infrared Spectrosc.* **2010**, *18*, 49–58. [CrossRef]
3. Ambrose, A.; Kandpal, L.M.; Kim, M.S.; Lee, W.-H.; Cho, B.-K. High speed measurement of corn seed viability using hyperspectral imaging. *Infrared Phys. Technol.* **2016**, *75*, 173–179. [CrossRef]
4. Sena, D.V.D.A.; Alves, E.U.; De Medeiros, D.S. Vigor tests to evaluate the physiological quality of corn seeds cv. 'Sertanejo'. *Cienci Rural* **2017**, *47*, 1678. [CrossRef]
5. Fessel, S.A.; Panobianco, M.; Vieira, R.D.; Da Cruz, M.C.P.; De Paula, R.C. Electrical conductivity testing of corn seeds as influenced by temperature and period of storage. *Pesqui. Agropecu. Bras.* **2006**, *41*, 1551–1559. [CrossRef]
6. Song, L.; Wang, Q.; Wang, C.; Lin, Y.; Yu, D.; Xu, Z.; Huang, Q.; Wu, Y. Effect of γ-irradiation on rice seed vigor assessed by near-infrared spectroscopy. *J. Stored Prod. Res.* **2015**, *62*, 46–51. [CrossRef]
7. Via, F.D.J.S.F.I.; Ivano, A.D.; Raniele, T.G.A.E.D.S.; Itamar, R.T.; Carlos, R.S. Physiological quality of quinoa seeds submitted to different storage conditions. *Afr. J. Agric. Res.* **2016**, *11*, 1299–1308. [CrossRef]
8. Nansen, C.; Zhao, G.; Dakin, N.; Zhao, C.; Turner, S.R. Using hyperspectral imaging to determine germination of native Australian plant seeds. *J. Photochem. Photobiol. B Biol.* **2015**, *145*, 19–24. [CrossRef]
9. Ropodi, A.; Panagou, E.; Nychas, G.-J. Data mining derived from food analyses using non-invasive/non-destructive analytical techniques; determination of food authenticity, quality & safety in tandem with computer science disciplines. *Trends Food Sci. Technol.* **2016**, *50*, 11–25. [CrossRef]
10. Xia, J.; Cao, H.; Yang, Y.; Zhang, W.; Wan, Q.; Xu, L.; Ge, D.; Zhang, W.; Ke, Y.; Huang, B. Detection of waterlogging stress based on hyperspectral images of oilseed rape leaves (*Brassica napus* L.). *Comput. Electron. Agric.* **2019**, *159*, 59–68. [CrossRef]
11. Díaz, J.J.V.; Aldana, A.P.S.; Zuluaga, D.V.R. Prediction of dry matter content of recently harvested 'Hass' avocado fruits using hyperspectral imaging. *J. Sci. Food Agric.* **2020**, *101*, 897–906. [CrossRef]
12. Tian, X.; Fan, S.X.; Huang, W.Q.; Wang, Z.L.; Li, J.B. Detection of early decay on citrus using hyperspectral transmittance imaging technology coupled with principal component analysis and improved watershed segmentation algorithms. *Postharvest Biol. Tech.* **2020**, *161*, 111071–111079. [CrossRef]
13. Ren, G.; Wang, Y.; Ning, J.; Zhang, Z. Evaluation of Dianhong black tea quality using near-infrared hyperspectral imaging technology. *J. Sci. Food Agric.* **2020**, *101*, 2135–2142. [CrossRef]
14. Hacisalihoglu, G.; Freeman, J.; Armstrong, P.R.; Seabourn, B.W.; Porter, L.D.; Settles, A.M.; Gustin, J.L. Protein, weight, and oil prediction by single-seed near-infrared spectroscopy for selection of seed quality and yield traits in pea (*Pisum sativum*). *J. Sci. Food Agric.* **2020**, *100*, 3488–3497. [CrossRef]
15. Bai, X.; Zhang, C.; Xiao, Q.; He, Y.; Bao, Y. Application of near-infrared hyperspectral imaging to identify a variety of silage maize seeds and common maize seeds. *RSC Adv.* **2020**, *10*, 11707–11715. [CrossRef]
16. Femenias, A.; Gatius, F.; Ramos, A.J.; Sanchis, V.; Marín, S. Standardisation of near infrared hyperspectral imaging for quantification and classification of DON contaminated wheat samples. *Food Control* **2019**, *111*, 107074. [CrossRef]
17. Kandpal, L.M.; Lohumi, S.; Kim, M.S.; Kang, J.-S.; Cho, B.-K. Near-infrared hyperspectral imaging system coupled with multivariate methods to predict viability and vigor in muskmelon seeds. *Sens. Actuators B Chem.* **2016**, *229*, 534–544. [CrossRef]
18. Li, Y.; Sun, J.; Wu, X.; Chen, Q.; Lu, B.; Dai, C. Detection of viability of soybean seed based on fluorescence hyperspectra and CARS-SVM-AdaBoost model. *J. Food Process. Preserv.* **2019**, *43*, e14238. [CrossRef]
19. Zhang, J.; Dai, L.; Cheng, F. Classification of Frozen Corn Seeds Using Hyperspectral VIS/NIR Reflectance Imaging. *Molecules* **2019**, *24*, 149. [CrossRef]
20. Kamilaris, A.; Prenafeta-Boldú, F.X. Deep learning in agriculture: A survey. *Comput. Electron. Agric.* **2018**, *147*, 70–90. [CrossRef]
21. Shen, D.; Wu, G.; Suk, H.-I. Deep Learning in Medical Image Analysis. *Annu. Rev. Biomed. Eng.* **2017**, *19*, 221–248. [CrossRef]
22. Zhu, S.; Zhou, L.; Gao, P.; Bao, Y.; He, Y.; Feng, L. Near-Infrared Hyperspectral Imaging Combined with Deep Learning to Identify Cotton Seed Varieties. *Molecules* **2019**, *24*, 3268. [CrossRef]
23. Feng, L.; Zhu, S.; Zhang, C.; Bao, Y.; Feng, X.; He, Y. Identification of Maize Kernel Vigor under Different Accelerated Aging Times Using Hyperspectral Imaging. *Molecules* **2018**, *23*, 3078. [CrossRef]
24. Zhang, T.; Wei, W.; Zhao, B.; Wang, R.; Li, M.; Yang, L.; Wang, J.; Sun, Q. A Reliable Methodology for Determining Seed Viability by Using Hyperspectral Data from Two Sides of Wheat Seeds. *Sensors* **2018**, *18*, 813. [CrossRef]

25. *GB 5009.3-2016*; Determination of Moisture in Food. General Administration of Quality Supervision. Inspection and Quarantine of the People's Republic of China: Beijing, China, 2016; Volume 1, pp. 1–2.
26. *GB 5009.6-2016*; Determination of Fat in Food. General Administration of Quality Supervision. Inspection and Quaran-tine of the People's Republic of China: Beijing, China, 2016; Volume 1, pp. 1–2.
27. *GB 5009.5-2016*; Determination of Protein in Food. General Administration of Quality Supervision. Inspection and Quarantine of the People's Republic of China: Beijing, China, 2016; Volume 1, pp. 1–5.
28. *GB 5009.9-2016*; Determination of Starch in Food. General Administration of Quality Supervision. Inspection and Quarantine of the People's Republic of China: Beijing, China, 2016; Volume 1, pp. 1–2.
29. Huo, Z.J.; Pan, X.L.; Li, J.Y. Problems and countermeasures in the operation of GB/T3543-1995 rules for agricultural seed testing. *Modern Agri.* **2004**, *1*, 14–15. [CrossRef]
30. ISTA. *International Rules for Seed Testing, International Seed Testing Association Chapter 1:1-12*; ISTA: Palmerston North, New Zealand, 2015.
31. Ru, C.; Li, Z.; Tang, R. A Hyperspectral Imaging Approach for Classifying Geographical Origins of Rhizoma Atractylodis Macrocephalae Using the Fusion of Spectrum-Image in VNIR and SWIR Ranges (VNIR-SWIR-FuSI). *Sensors* **2019**, *19*, 2045. [CrossRef]
32. Wu, D.; He, Y.; Feng, S.; Sun, D.-W. Study on infrared spectroscopy technique for fast measurement of protein content in milk powder based on LS-SVM. *J. Food Eng.* **2008**, *84*, 124–131. [CrossRef]
33. Gerhardt, N.; Schwolow, S.; Rohn, S.; Pérez-Cacho, P.R.; Galán-Soldevilla, H.; Arce, L.; Weller, P. Quality assessment of olive oils based on temperature-ramped HS-GC-IMS and sensory evaluation: Comparison of different processing approaches by LDA, kNN, and SVM. *Food Chem.* **2019**, *278*, 720–728. [CrossRef]
34. Qiu, G.; Lü, E.; Wang, N.; Lu, H.; Wang, F.; Zeng, F. Cultivar Classification of Single Sweet Corn Seed Using Fourier Transform Near-Infrared Spectroscopy Combined with Discriminant Analysis. *Appl. Sci.* **2019**, *9*, 1530. [CrossRef]
35. Fraiwan, L.; Lweesy, K.; Khasawneh, N.; Wenz, H.; Dickhaus, H. Automated sleep stage identification system based on time–frequency analysis of a single EEG channel and random forest classifier. *Comput. Methods Programs Biomed.* **2012**, *108*, 10–19. [CrossRef]
36. Jiao, C.; Chen, C.; McGarvey, R.G.; Bohlman, S.; Jiao, L.; Zare, A. Multiple instance hybrid estimator for hyperspectral target characterization and sub-pixel target detection. *ISPRS J. Photogramm. Remote. Sens.* **2018**, *146*, 235–250. [CrossRef]
37. Chen, L.-C.; Papandreou, G.; Kokkinos, I.; Murphy, K.; Yuille, A.L. DeepLab: Semantic Image Segmentation with Deep Convolutional Nets, Atrous Convolution, and Fully Connected CRFs. *IEEE Trans. Pattern Anal. Mach. Intell.* **2018**, *40*, 834–848. [CrossRef]
38. Zhong, L.; Guo, X.; Xu, Z.; Ding, M. Soil properties: Their prediction and feature extraction from the LUCAS spectral library using deep convolutional neural networks. *Geoderma* **2021**, *402*, 115366. [CrossRef]
39. Li, J.; Tian, X.; Huang, W.; Zhang, B.; Fan, S. Application of long-wave near infrared hyperspectral imaging for measurement of color distribution in salmon fillet. *Food Anal. Methods* **2016**, *9*, 3087–3098. [CrossRef]
40. Williams, P.J.; Kucheryavskiy, S. Classification of maize kernels using NIR hyperspectral imaging. *Food Chem.* **2016**, *209*, 131–138. [CrossRef]
41. Liu, D.; Sun, D.-W.; Zeng, X.-A. Recent Advances in Wavelength Selection Techniques for Hyperspectral Image Processing in the Food Industry. *Food Bioprocess Technol.* **2013**, *7*, 307–323. [CrossRef]
42. Peng, Y.K.; Zhao, F.; Li, L.; Xing, Y.Y.; Fang, X.Q. Discrimination of heat-damaged tomato seeds based on near infrared spectroscopy and PCA-SVM method. *Trans. Chin. Soc. Agric. Eng.* **2018**, *34*, 159–165. [CrossRef]
43. Wu, N.; Zhang, Y.; Na, R.; Mi, C.; Zhu, S.; He, Y.; Zhang, C. Variety identification of oat seeds using hyperspectral imaging: Investigating the representation ability of deep convolutional neural network. *RSC Adv.* **2019**, *9*, 12635–12644. [CrossRef]
44. Zhu, S.; Zhou, L.; Zhang, C.; Bao, Y.; Wu, B.; Chu, H.; Yu, Y.; He, Y.; Feng, L. Identification of Soybean Varieties Using Hyperspectral Imaging Coupled with Convolutional Neural Network. *Sensors* **2019**, *19*, 4065. [CrossRef]
45. Fu, J.R. *Seed Physiology*; Science Press: Beijing, China, 1985.
46. Taiz, L.; Jones, R.L. Gibberellic acid, beta-1,3-glucanase and the cell walls of barley aleurone layers. *Planta* **1970**, *92*, 73–84. [CrossRef]
47. Hara-Nishimura, I.; Nishimura, M.; Daussant, J. Conversion of free β-amylase to bound β-amylase on starch granules in the barley endosperm during desiccation phase of seed development. *Protoplasma* **1986**, *134*, 149–153. [CrossRef]
48. Yong-Qiang, M.A.; Han, C.R. *Changes of Starch in Corn during Germination*; Grain Processing: Muscatine County, IA, USA, 2007.
49. Chavan, J.K.; Kadam, S.S.; Salunkhe, D.K. Changes in Tannin, Free Amino Acids, Reducing Sugars, and Starch During Seed Germination of Low and High Tannin Cultivars of Sorghum. *J. Food Sci.* **1981**, *46*, 638–639. [CrossRef]
50. Zhang, Y.; Li, Y.; Song, J.; Chen, X.; Lu, Y.; Wang, W. Pearson correlation coefficient of current derivatives based pilot protection scheme for long-distance LCC-HVDC transmission lines. *Int. J. Electr. Power Energy Syst.* **2020**, *116*, 105526. [CrossRef]
51. Yang, G.; Wang, Q.; Liu, C.; Wang, X.; Fan, S.; Huang, W. Rapid and visual detection of the main chemical compositions in maize seeds based on Raman hyperspectral imaging. *Spectrochim. Acta Part A Mol. Biomol. Spectrosc.* **2018**, *200*, 186–194. [CrossRef]
52. Feng, X.; Peng, C.; Chen, Y.; Liu, X.; Feng, X.; He, Y. Discrimination of CRISPR/Cas9-induced mutants of rice seeds using near-infrared hyperspectral imaging. *Sci. Rep.* **2017**, *7*, 15934–15943. [CrossRef]